3D single-cell shape analysis of cancer cells using geometric deep learning

Anonymous Author(s)
Affiliation
Address
email

Abstract

Aberrations in the 3D geometry of biological cells are linked to disease, and advances in microscopy have lead to rapid growth in 3D cell imaging. Despite this, there is a paucity of methods to quantify 3D cell shapes. Currently most descriptions of cell geometry use predefined mathematical measures, rather than data-driven approaches. To address this we have adapted existing geometric deep learning and improved deep embedded clustering (IDEC), and present a novel dynamic graph convolutional foldingnet autoencoder (DGCNN) with IDEC to simultaneously learn lower-dimensional representations and classes of 3D cell shapes from a dataset of more than 70,000 drug-treated melanoma cells imaged by 3D light-sheet microscopy. We propose to describe cell shape using 3D quantitative morphological signatures (3DQMS), which represent a cell's similarity to shape modes in the dataset. This lead to the insight that drugs treated with similar inhibitors share morphological signatures, and that morphological signatures can be used to predict the activity of a drug. We also found that our model improves upon existing methods for problems such as classifying cell types based on geometry, by using a recently published dataset of 3D red blood cells. This suggests that our features generalise across datasets, and that our geometric deep learning models are capturing features which are not explained by classical measures of shape. Finally, we highlight the implementation of our framework as a python software package for ease of use by the medical research community.

1 Introduction

Aberrations in cell geometry are linked to cell signalling and disease. For example, metastatic melanoma cells alter their shape to invade tissues and drive disease [1]. Traditionally, we understand shape using predetermined or "classical" features. These are pre-selected, measures of cell geometry and often require a preconceived idea of which features are important. These descriptors include region-based shape descriptors such as area, perimeter, and eccentricity [2, 3, 4, 5, 6], as well as boundary features such as the relative position of consecutive points along a 2D perimeter [7, 8]. In the context of studying living cells in 2D images, these geometric approaches have been successful at identifying major categories of cell shape, and linking cell shapes to the molecular signalling pathways that control geometry [9, 1, 10], or respond to changes in geometry [11, 12, 13, 14].

While measuring shape in 2D images has been illuminating, cells exist in 3D environments, and their 3D geometry is a rich source of information about the inner workings of cells and tissues. For example, recent pioneering work has demonstrated that shape motifs extracted from 3D images can be linked to lipid membrane signalling and cancer signalling pathways [11], and changes in 3D nuclear morphometry are linked to chromatin organisation [15]. At the scale of developing tissues,

Submitted to 36th Conference on Neural Information Processing Systems (NeurIPS 2022). Do not distribute.

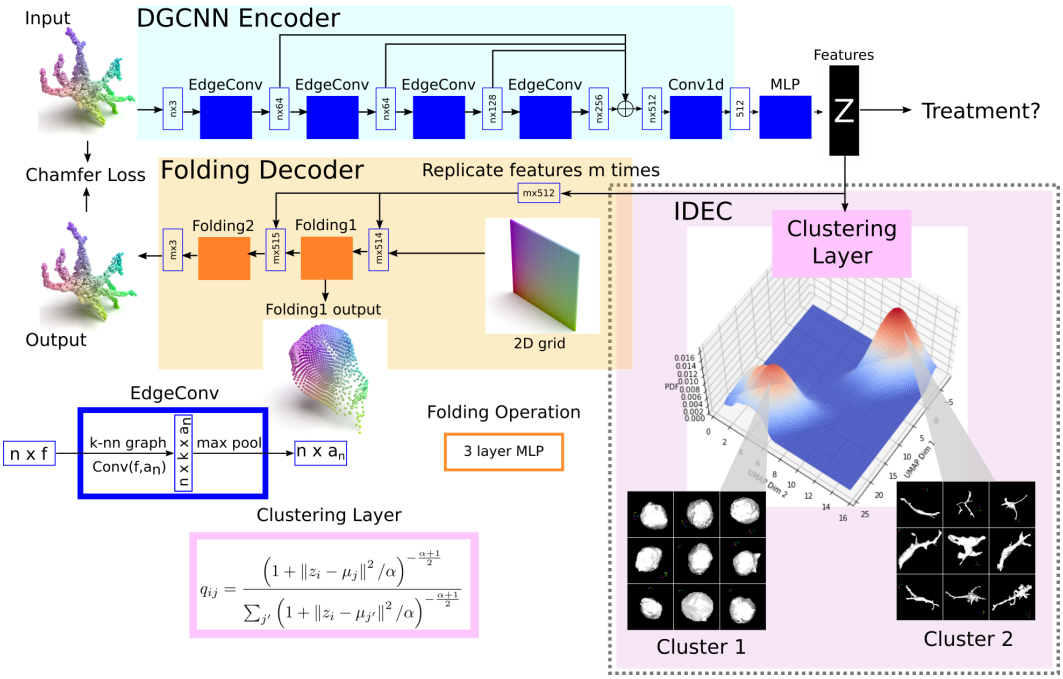

Figure 1: **DFN architecture.** DFN comprises of a DGCNN encoder and a FoldingNet decoder. We add a clustering layer in the form of IDEC.

the discovery of new 3D geometries has explained how cells pack stably into curved organs [16]. Now, the development of high throughput light-sheet imaging [17, 18] has made it possible to image large numbers of cells in 3D with sub-cellular resolution. This development has led to a growing need for accurate 3D shape representations.

We have addressed this need using unsupervised geometric deep learning to learn shape representations of cells from 3D microscopy images of metastatic melanoma cells embedded in collagen tissue-like matrices. We have segmented segmented these 3D single cells, used marching-cubes to create mesh objects and then sampled 2048 points from the surfaces of the meshes to obtain point cloud representation of each cell and nuclei (See Appendix A). We utilised a combination of state-of-the-art existing learning methods. We used a dynamic graph convolutional foldingnet autoencoder (DFN) with improved deep embedded clustering to simultaneously learn lower-dimensional representations and classes of 3D cell shapes from a dataset of more than 70,000 drug-treated melanoma cells imaged by high throughput light-sheet microscopy. We then apply the learned model to different datasets to show improved accuracies of blood cell shape classification than when using classical features and spherical harmonics. Finally, we have packaged our software in an easy-to-use Python package to encourage open science.

2 Methods

2.1 Dynamic graph convolutional foldingnet

The DFN follows the design of the FoldingNet [19] with a dynamic graph convolutional neural netowork (DGCNN) [20] as the encoder. This encoder takes a 3D point cloud as input, constructs a local neighbourhood graph on these points and applies convolution-like operations on the edges of connecting neighbouring points. This outputs a lower dimensional representation of the input point cloud. The FoldingNet decoder then takes this representation, concatenates it to points sampled from a plane and passes it through two folding operations to reconstruct the input point cloud. We use an extended Chamfer Distance (CD) defined in [19] as our reconstruction criterion.

2.2 Improved deep embedded clustering

Deep embedded clustering (DEC) [21] is a specialised clustering technique that simultaneously learns feature representations and cluster assignments using autoencoders. Following the algorithm described in [21], we propose learning autoencoder parameters θ which map the 3D shapes into embedded feature space $\mathbf{Z}$ as well as k_c cluster centres $\{\mu_j \in Z\}_{j=1}^{k_c}$ of the embedded feature space $\mathbf{Z}$. The clustering layer then assigns soft-labels (q_{ij}) to each input by mapping features to clusters based on the Student's t-distribution as a kernel that represents the similarity between a feature vector ($\mathbf{z_i}$) and a cluster centre (μ_j). This can be interpreted as the probability of assigning input cell shape i to cluster j, hence why this is a soft assignment. Soft-assignments with high probabilities are considered trustworthy and thus DEC designs a target distribution which raises this to the second power to place more emphasis on these confident assignments. The features at cluster centres become representations of 'example' shapes of each shape class. For example, if there are k_c clusters in the dataset, each cell is assigned k_c soft-labels (one for each cluster) and each soft-label contains scores from zero to one reflecting how similar the cell is to each of the different cluster centres (with a values of one being most similar). Since the 3D shape of cells in a fixed assay is a continuous distribution with an indefinite number of distinct classes (cells may be very similar in shape, yet almost never the exact same), it is more natural to describe a shape by a signature of how similar it is to a number of different exemplar classes. For example, we may wish to describe the 3D shape of a cell to be 30% similar to shape cluster 0, 10% similar to shape cluster 1, 5% similar to shape cluster 2 for shape classes $j = 0, 1, ...k_c$, such that the sum of similarity percentages add to 100 ($\sum_{j=0}^{k_c} k_c^{(j)} = 100$, where $k_c^{(j)}$ is shape class j). This can be defined as a quantitative morphological signature for the 3D shape of a cell (3DQMS). Therefore, our k_c-dimensional vector of soft-labels can be used as a 3DQMS. [21] proposed pre-training an autoencoder and then disregarding the decoder part and replacing it with the clustering layer, but [22, 23] showed this weakens the representitativeness of the features learned. Improved deep embedded clustering (IDEC) [24] proposed adding the decoder back to the second phase of training to optimise both the reconstruction loss and the clustering loss simultaneously. We followed IDEC [24].

3 Results

3.1 Learned shape features predict drug treatment with greater accuracy than previous approaches

Many studies in computer vision and 3D shape representation learning test the effectiveness of their representations with downstream classification tasks. This involves using a trained model to extract features from a dataset and then using these features to train a linear support vector machine (SVM) classifier [19, 25, 26, 27]. These tasks generally involve classification between objects from distinct semantic classes [28]. Our dataset is comprised of a single cell type and did not have such distinct semantic classes, so to test our shape representations, we predicted our drug treatment labels. Following similar procedures to previous researchers [19, 25, 26, 27], we used the trained DFN without the addition of the clustering layer to extract features from each cell. These features were then used to train a linear SVM. For all experiments, we use one-versus-one SVM classifiers with an L2 penalty (C = 1), balanced class weights, and intercept scaling during training. We performed 10-fold cross-validation for each experiment and report mean accuracies. We found the greatest prediction accuracy resulted from combining both cytoplasmic and nuclear shape features, with predictions up to 89% for cells treated with myosin inhibitors and microtubule inhibitors. This is apposed to an accuracy of 82% when using classical features. Furthermore, we tested whether prediction accuracies were effected by a cells environment (closer to the coverslip - in a rigid environment - or further away from the coverslip - in a more tissue-like environment). Higher accuracies were seen in cells that were closer to the coverslip.

3.2 Improved deep embedded clustering learns a 3D quantitative morphological signature that generates new biological insights

After training the DFN autoencoder to learn 3D cell shape representation, we performed improved deep embedded clustering (IDEC) [24] to learn the 3DQMS of every cell. The number of clusters was

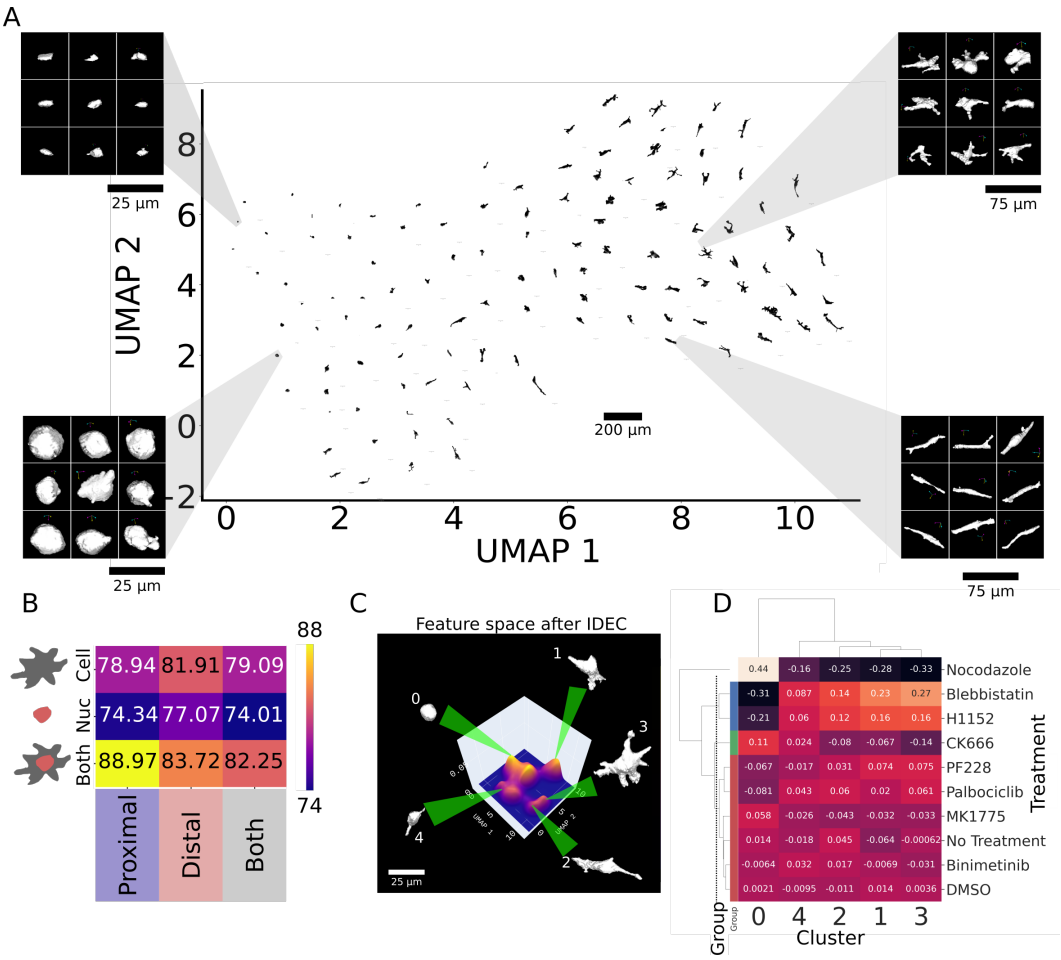

Figure 2: **Using DFN to explore the cell shape landscape, predict small molecule treatment and link drugs acting in the same pathway. (A) shows the cell shape landscape of the metastatic melanoma cells. (B)**

chosen as a hyper-parameter. However, this could also be estimated by prior knowledge, or through more formal methods such as the elbow, average silhouette or gap statistic methods when undertaking the initial k-means clustering. We examined the 3DQMS for cells treated with different inhibitors to show how these inhibitors effect the shapes that cells can take on. Blebbistatin treated cells had high scores for protrusive shape classes with Nocodazole treated cells having high scores for the round shape class. Furthermore, we noted that two distinct inhibitors of myosin activation (Blebbistatin and H1152) grouped together, indicating that the 3DQMS will be a powerful tool for using cell shape to identify drugs that act on similar pathways. The other classes of treatment effects on shape included Nocodazole, which inhibits the polymerisation of microtubules, CK666, which prevents actin branching and then control cells grouped with those treatments that do not have significant effects on cell shape.

3.3 DFN features outperform other features on 3D blood cell shapes classification

To prove the generalisability of our methods, we extend them to other datasets. The first dataset is a recently published library of 825 3D red blood cell shapes [29]. First, works in [29] extracted 3D shape descriptors using spherical harmonics and then used these features to train a multi-layered perceptron to classify 3D red blood cell shape. They achieved an accuracy of 97.3%. Secondly, works in [30] extract 126 "classical" features from the 3D shapes of the red blood cells, comprising of a volume, roughness convexity and gabor features. They then use these features to train a random forest classifier to predict the 3D red blood cell shape classes. They achieved a highest F1-score of 88.6%

(with a standard deviation of 3.7% using 10-fold cross validation). When we used our methods to classify the six classes (with the SDE group) we achieved a mean accuracy of 99.52% (standard deviation of 0.18%) and a mean weighted F1-score of 99.53% (with a standard deviation of 0.18%). Using our features to classify 3D red blood cell shapes has significantly outperformed both spherical harmonics and several commonly used classical measures of cell geometry.

4 Conclusion

Here, we have utilised a combination of state-of-the-art computer vision techniques and applied it to cancer biology. We have learned the shape representations of 3D cancer cells using geometric deep learning and have shown that these outperform traditional measures of cell shape when predicting drug treatment as well as shape classes. We propose defining cell shapes by their similarity to shape modes in the dataset - known as their 3DQMS - and show that this is useful in linking treatments which effect the same pathway. We also found strikingly similar deep learning shape signatures between cells treated with microtubule polymerisation inhibitors and branched actin inhibitors. Finally, we implemented our methods as a Python package for ease of use by the research community.

References

[1] Pei-Hsun Wu, Daniele M. Gilkes, Jude M. Phillip, Akshay Narkar, Thomas Wen-Tao Cheng, Jorge Marchand, Meng-Horng Lee, Rong Li, and Denis Wirtz. Single-cell morphology encodes metastatic potential. *Science Advances*, 6(4):eaaw6938, January 2020. Publisher: American Association for the Advancement of Science.

[2] Veronika Graml, Xenia Studera, Jonathan L.D. Lawson, Anatole Chessel, Marco Geymonat, Miriam Bortfeld-Miller, Thomas Walter, Laura Wagstaff, Eugenia Piddini, and Rafael E. Carazo-Salas. A genomic multiprocess survey of machineries that control and link cell shape, microtubule organization, and cell-cycle progression. *Developmental Cell*, 31(2):227–239, 2014.

[3] Saurav Basu, Soheil Kolouri, and Gustavo K. Rohde. Detecting and visualizing cell phenotype differences from microscopy images using transport-based morphometry. *Proceedings of the National Academy of Sciences*, 111(9):3448–3453, 2014.

[4] Thouis R. Jones, Anne E. Carpenter, Michael R. Lamprecht, Jason Moffat, Serena J. Silver, Jennifer K. Grenier, Adam B. Castoreno, Ulrike S. Eggert, David E. Root, Polina Golland, and David M. Sabatini. Scoring diverse cellular morphologies in image-based screens with iterative feedback and machine learning. *Proceedings of the National Academy of Sciences*, 106(6):1826–1831, 2009.

[5] Chris Bakal, John Aach, George Church, and Norbert Perrimon. Quantitative morphological signatures define local signaling networks regulating cell morphology. *Science (New York, N.Y.)*, 316(5832):1753–1756, June 2007. Number: 5832.

[6] Zheng Yin, Amine Sadok, Heba Sailem, Afshan McCarthy, Xiaofeng Xia, Fuhai Li, Mar Arias Garcia, Louise Evans, Alexis R. Barr, Norbert Perrimon, Christopher J. Marshall, Stephen T. C. Wong, and Chris Bakal. A screen for morphological complexity identifies regulators of switch-like transitions between discrete cell shapes. *Nature Cell Biology*, 15(7):860–871, July 2013.

[7] Pei-Hsun Wu, Jude M. Phillip, Shyam B. Khatau, Wei-Chiang Chen, Jeffrey Stirman, Sophie Rosseel, Katherine Tschudi, Joshua Van Patten, Michael Wong, Sonal Gupta, Alexander S. Baras, Jeffrey T. Leek, Anirban Maitra, and Denis Wirtz. Evolution of cellular morpho-phenotypes in cancer metastasis. *Scientific Reports*, 5(1):18437, 2015.

[8] Jude M. Phillip, Kyu-Sang Han, Wei-Chiang Chen, Denis Wirtz, and Pei-Hsun Wu. A robust unsupervised machine-learning method to quantify the morphological heterogeneity of cells and nuclei. *Nature Protocols*, 16(2):754–774, Feb 2021.

[9] Sam Cooper, Amine Sadok, Vicky Bousgouni, and Chris Bakal. Apolar and polar transitions drive the conversion between amoeboid and mesenchymal shapes in melanoma cells. *Molecular biology of the cell*, 26(22):4163–4170, 11 2015.

[10] Erik Sahai and Christopher J. Marshall. Differing modes of tumour cell invasion have distinct requirements for Rho/ROCK signalling and extracellular proteolysis. *Nature Cell Biology*, 5(8):711–719, August 2003.

[11] Meghan K. Driscoll, Erik S. Welf, Andrew R. Jamieson, Kevin M. Dean, Tadamoto Isogai, Reto Fiolka, and Gaudenz Danuser. Robust and automated detection of subcellular morphological motifs in 3D microscopy images. *Nature Methods*, 16(10):1037–1044, October 2019.

[12] Julia E. Sero, Heba Zuhair Sailem, Rico Chandra Ardy, Hannah Almuttaqi, Tongli Zhang, and Chris Bakal. Cell shape and the microenvironment regulate nuclear translocation of NF-B in breast epithelial and tumor cells. *Molecular Systems Biology*, 11(3):790, March 2015.

[13] Julia E. Sero and Chris Bakal. Multiparametric Analysis of Cell Shape Demonstrates that -PIX Directly Couples YAP Activation to Extracellular Matrix Adhesion. *Cell Systems*, 4(1):84–96.e6, January 2017. Number: 1.

[14] Patricia Pascual-Vargas, Samuel Cooper, Julia Sero, Vicky Bousgouni, Mar Arias-Garcia, and Chris Bakal. RNAi screens for Rho GTPase regulators of cell shape and YAP/TAZ localisation in triple negative breast cancer. *Scientific Data*, 4:170018, March 2017.

[15] Alexandr A. Kalinin, Xinhai Hou, Alex S. Ade, Gordon-Victor Fon, Walter Meixner, Gerald A. Higgins, Jonathan Z. Sexton, Xiang Wan, Ivo D. Dinov, Matthew J. O'Meara, and Brian D. Athey. Valproic acid-induced changes of 4D nuclear morphology in astrocyte cells. *Molecular Biology of the Cell*, 32(18):1624–1633, August 2021. Publisher: American Society for Cell Biology (mboc).

[16] Pedro Gómez-Gálvez, Pablo Vicente-Munuera, Antonio Tagua, Cristina Forja, Ana M. Castro, Marta Letrán, Andrea Valencia-Expósito, Clara Grima, Marina Bermúdez-Gallardo, Óscar Serrano-Pérez-Higueras, Florencia Cavodeassi, Sol Sotillos, María D. Martín-Bermudo, Alberto Márquez, Javier Buceta, and Luis M. Escudero. Scutoids are a geometrical solution to three-dimensional packing of epithelia. *Nature Communications*, 9(1):1–14, July 2018. Number: 1 Publisher: Nature Publishing Group.

[17] C. Dunsby. Optically sectioned imaging by oblique plane microscopy. *Optics Express*, 16(25):20306–20316, December 2008.

[18] Vincent Maioli, George Chennell, Hugh Sparks, Tobia Lana, Sunil Kumar, David Carling, Alessandro Sardini, and Chris Dunsby. Time-lapse 3-d measurements of a glucose biosensor in multicellular spheroids by light sheet fluorescence microscopy in commercial 96-well plates. *Scientific Reports*, 6(1):37777, Nov 2016.

[19] Yaoqing Yang, Chen Feng, Yiru Shen, and Dong Tian. Foldingnet: Point cloud auto-encoder via deep grid deformation, 2018.

[20] Yue Wang, Yongbin Sun, Ziwei Liu, Sanjay E. Sarma, Michael M. Bronstein, and Justin M. Solomon. Dynamic graph cnn for learning on point clouds. *ACM Transactions on Graphics (TOG)*, 2019.

[21] Junyuan Xie, Ross Girshick, and Ali Farhadi. Unsupervised deep embedding for clustering analysis. In Maria Florina Balcan and Kilian Q. Weinberger, editors, *Proceedings of The 33rd International Conference on Machine Learning*, volume 48 of *Proceedings of Machine Learning Research*, pages 478–487, New York, New York, USA, 20–22 Jun 2016. PMLR.

[22] Xifeng Guo, Xinwang Liu, En Zhu, and Jianping Yin. Deep clustering with convolutional autoencoders. In Derong Liu, Shengli Xie, Yuanqing Li, Dongbin Zhao, and El-Sayed M. El-Alfy, editors, *Neural Information Processing*, pages 373–382, Cham, 2017. Springer International Publishing.

[23] Xifeng Guo, En Zhu, Xinwang Liu, and Jianping Yin. Deep embedded clustering with data augmentation, 14–16 Nov 2018.

[24] Xifeng Guo, Long Gao, Xinwang Liu, and Jianping Yin. Improved deep embedded clustering with local structure preservation. In *Proceedings of the Twenty-Sixth International Joint Conference on Artificial Intelligence, IJCAI-17*, pages 1753–1759, 2017.

[25] Ling Zhang and Zhigang Zhu. Unsupervised feature learning for point cloud by contrasting and clustering with graph convolutional neural network, 2019.

[26] Xiang Gao, Wei Hu, and Guo-Jun Qi. GraphTER: Unsupervised learning of graph transformation equivariant representations via auto-encoding node-wise transformations. In *Proceedings of the IEEE Conference on Computer Vision and Pattern Recognition (CVPR)*, June 2020.

[27] Juyoung Yang, Pyunghwan Ahn, Doyeon Kim, Haeil Lee, and Junmo Kim. Progressive seed generation auto-encoder for unsupervised point cloud learning. In *Proceedings of the IEEE/CVF International Conference on Computer Vision (ICCV)*, pages 6413–6422, October 2021.

[28] Zhirong Wu, Shuran Song, Aditya Khosla, Fisher Yu, Linguang Zhang, Xiaoou Tang, and Jianxiong Xiao. 3d shapenets: A deep representation for volumetric shapes, 2014.

[29] Greta Simionato, Konrad Hinkelmann, Revaz Chachanidze, Paola Bianchi, Elisa Fermo, Richard van Wijk, Marc Leonetti, Christian Wagner, Lars Kaestner, and Stephan Quint. Red blood cell phenotyping from 3d confocal images using artificial neural networks. *PLOS Computational Biology*, 17(5):1–17, 05 2021.

[30] Dominik J. E. Waibel, Niklas Kiermeyer, Scott Atwell, Ario Sadafi, Matthias Meier, and Carsten Marr. Shapr predicts 3d cell shapes from 2d microscopic images. *bioRxiv*, 2022.

A Appendix

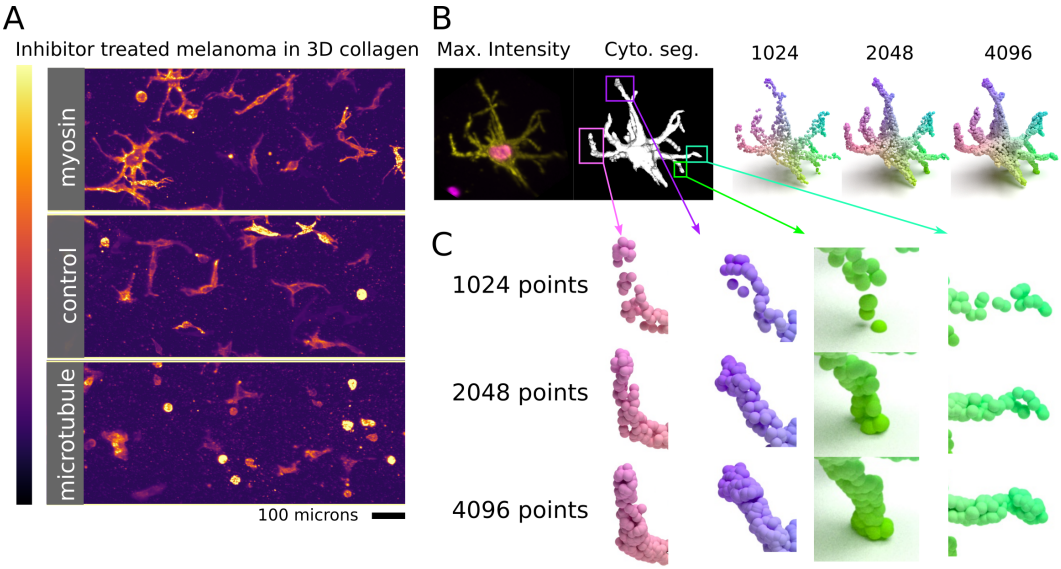

Figure 3: (A) Single-cells embedded in a collagen matrix were treated with a variety of small molecule drugs and imaged in 3D in high-throughput by stage scanning oblique plane microscopy (ssOPM). Maximum intensity projections (XY view) of cells treated with DMSO (control), Blebbistatin (myosin) and Nocodazole (microtubule) are shown. Intensity is the grayscale intensity of the CAAX-GFP membrane marker. (B) The cells were labelled with transgenes expressing Histone-2B (which labels the nucleus) and CAAX-GFP (which labels cell membranes). Nucleus and cell label intensities (Max. Intensity) and the cytoplam segmentation masks (Cyto. seg.) are shown for a single cell. We used the marching cubes algorithm to create a mesh object of vertices, faces, and normals and then sampled 1048, 2048, and 4096 points from this mesh object to create a point cloud for each cell cytoplasm and nucleus. (C) We found that 2046 points was dense enough to represent the shape while being computationally efficient.